



An algorithm to minimize errors in displacement measurements via double integration of noisy acceleration signals

José Geraldo Telles Ribeiro¹ · Jaime Tupiassú Pinho de Castro² · Marco Antonio Meggiolaro²

Received: 19 June 2020 / Accepted: 1 July 2021
© The Brazilian Society of Mechanical Sciences and Engineering 2021

Abstract

This paper presents analyses of noise effects in displacement histories measured by double numerical integration of acceleration data. Since such noise-induced errors tend to be highly random, they must be estimated statistically. The noise root mean square (RMS) value can be used to estimate its effect on the actual resolution of acceleration measurements, and a good low-pass filter can improve this resolution. This RMS value can be estimated by multiplying the noise density by the square root of the cutoff frequency of the filter used. However, this information alone cannot estimate the displacement resolution directly. To mitigate this problem, this study proposes suitable parameters to estimate the error induced in displacements measured by double integration of noisy acceleration data and shares a code that can be used to minimize such errors.

Keywords Double integration · Acceleration-measured displacements · Noise · Displacement resolution

1 Introduction

The measurement of displacements is a particularly important task in many structural engineering applications, from monitoring ground motions during earthquakes to structural integrity evaluations of huge structures, such as dams and stadiums. An emerging area is the monitoring of tall buildings [1] and long-span bridges [2], which are very sensitive to wind loads. However, it can be difficult or even impossible to use non-inertial gauges based on linear variable differential transforms (LVDT), eddy current, capacitive, or resistive sensors, or else on laser Doppler vibrometers or other optical sensors to directly measure displacements. All such non-inertial displacement gauges need a motionless reference,

which in many if not most cases simply may be unavailable in practice.

The double integration of inertial accelerometer signals seems a simple natural choice in such common cases, but this apparently trivial methodology may introduce many error sources that can severely degrade or even spoil the calculated displacements, if not properly dealt with. Among them, a trend or bias proportional to the measurement time t caused by unknown initial conditions, a second trend proportional to t^2 caused by zero shifts in the integration circuits [3–6], and a third trend proportional to $t^{3/2}$ caused by the noise associated to the acceleration measurements [7–9].

All these error trends affect the low-frequency components of the calculated displacements and can severely reduce the accuracy of their peak values, which are most important for structural integrity analyses. Indeed, static damage mechanisms are driven by peak strains or stresses, which are also the second driving force for fatigue damage (the other is the strain/stress range). Some instrumentation systems use accelerometers and global positioning systems (GPS) [10–14] to mitigate this problem, but such a solution is not feasible in many practical cases, because the resolution of commercially available GPS simply is not enough to allow accurate strain calculations from the measured displacements in most cases. Therefore, displacement measurement systems based only on inertial acceleration signals still are the desired choice in many, if not most, practical

Technical Editor: Monica Carvalho.

✉ José Geraldo Telles Ribeiro
jose.ribeiro@uerj.br

Jaime Tupiassú Pinho de Castro
jtcastro@puc-rio.br

Marco Antonio Meggiolaro
meggi@puc-rio.br

¹ Mechanical Engineering Department, Rio de Janeiro State University, Rio de Janeiro, RJ, Brazil

² Mechanical Engineering Department, Catholic University of Rio de Janeiro, Rio de Janeiro, RJ, Brazil

applications. Recent works study methods to decrease double integration errors of acceleration data without using data fusion with GPS [10–20], but all such methods still have some limitations [21].

The FFT-DDI (fast Fourier transform—displacement double integration) method developed by Ribeiro et al. [22] has some promising intrinsic features, which are used and further explored in this paper. However, since the FFT-DDI development cannot be replicated here, that work should be consulted as needed. The FFT-DDI can remove zero shifts of integrated signals in the frequency domain, using the information of the real part of the first frequency components identified on the FFT of the signal. Such components are then used to estimate the value of the static or 0 Hz signal component, which can much affect displacement peaks and is the only frequency component that is modified. In this way, this method intrinsically avoids time aliasing induced by digital filtering in the time domain [23–25], as well as the limitations of least squares data-fitting procedures.

However, since this method does not use a high-pass finite impulse response (FIR) filter, it is sensitive to acceleration noise. The high-pass filter must be used because the integration process is extremely sensitive to low-frequency components. The zero mean random walk with a standard deviation proportional to $t^{3/2}$ is removed [24], but the remaining frequency components that are not modified can introduce random errors that reduce the actual resolution of the measured displacements, affecting both their RMS and peak values. Aiming to quantify such problems, this paper presents an analysis of how acceleration noise affects displacement measurements and elaborates suitable parameters to estimate this error when using the FFT-DDI. These objectives are accomplished in four steps:

- In Sect. 2, by deducing a general formula to estimate the error introduced by acceleration noise in calculated velocities and displacements.
- In Sect. 3, by validating the equation deduced in Sect. 2 through numerical simulations.
- In Sect. 4, by testing the general formula in experimental measurements.
- In Sect. 5, presenting the resulting algorithm to minimize displacement errors when using the FFT-DDI method detailed in Appendix 2.

2 Acceleration noise effects

If the noise in the acceleration signal is Gaussian white, its variance can estimate its intrinsic error. Therefore, the errors in velocity and displacement measurements based on the numerical integration of noisy acceleration signals depend on their variances too.

The objective of this section is to present an analysis of the effect of acceleration noise in the velocity and displacement signals obtained by numerically integrating that signal. This effect does not depend on the integration procedure and is always present, leading to the necessity of using a high-pass filter in many practical situations.

Since variances and power spectra are related by Parseval's theorem, it can be used to estimate noise effects, as described in the following subsections.

2.1 Residual noise of the acceleration signal

For simulation purposes, it is necessary to integrate noisy acceleration samples, which have been generated in this work by using the algorithm shown in Appendix 1. Figure 1 shows 1000 noise samples, with $N = 8192$ points each, of the acceleration signal filtered using a 2-pole Butterworth anti-aliasing filter with a cutoff frequency $f_c = 250$ Hz, along with their mean power spectrum. These signals have been generated considering an acceleration noise density $N_d = 190 \mu\text{g}/\sqrt{\text{Hz}}$ and a sample frequency $f_s = 1612.9$ Hz.

The estimated variance $\hat{\sigma}_a^2$ of the accelerometer noise can be related to its power spectrum using Parseval's equality, as shown in Eq. (1) [26], where N is the number of samples, $A(n)$ is the FFT of the acceleration noise, and $P_{aa}(n)$ is its power spectrum.

$$\hat{\sigma}_a^2 = \frac{1}{N} \sum_{k=1}^N [a(k)]^2 = \sum_{n=1}^N P_{aa}(n) = \sum_{n=1}^N A(n) * \overline{A(n)}. \quad (1)$$

The accelerometer noise density N_d is the square root of the power spectral density in the bandwidth B_a of its noise output, which is measured in $\mu\text{g}/\sqrt{\text{Hz}}$ and can be estimated using Eq. (2).

$$N_d = \hat{\sigma}_a / \sqrt{B_a}. \quad (2)$$

Then, the RMS value of the accelerometer noise output can be obtained by multiplying this value by the square root of the measurement bandwidth. This is a good estimate of the accelerometer resolution, since accelerations below this RMS value cannot be separated from the signal noise. These data are (or should be) provided by the accelerometer manufacturer. Considering that the original signal noise (before filtering) can be considered white Gaussian, its mean power spectrum is flat over all frequencies, hence a constant P_{aa} value can be estimated using:

$$P_{aa} \approx \frac{\hat{\sigma}_a^2}{N} = N_d^2 \cdot \frac{f_s}{2N} = \frac{N_d^2}{2N\Delta t} = \frac{N_d^2}{2T}. \quad (3)$$

Since the value of the power spectrum P_{aa} is not modified by low-pass filtering of the frequencies below its cutoff

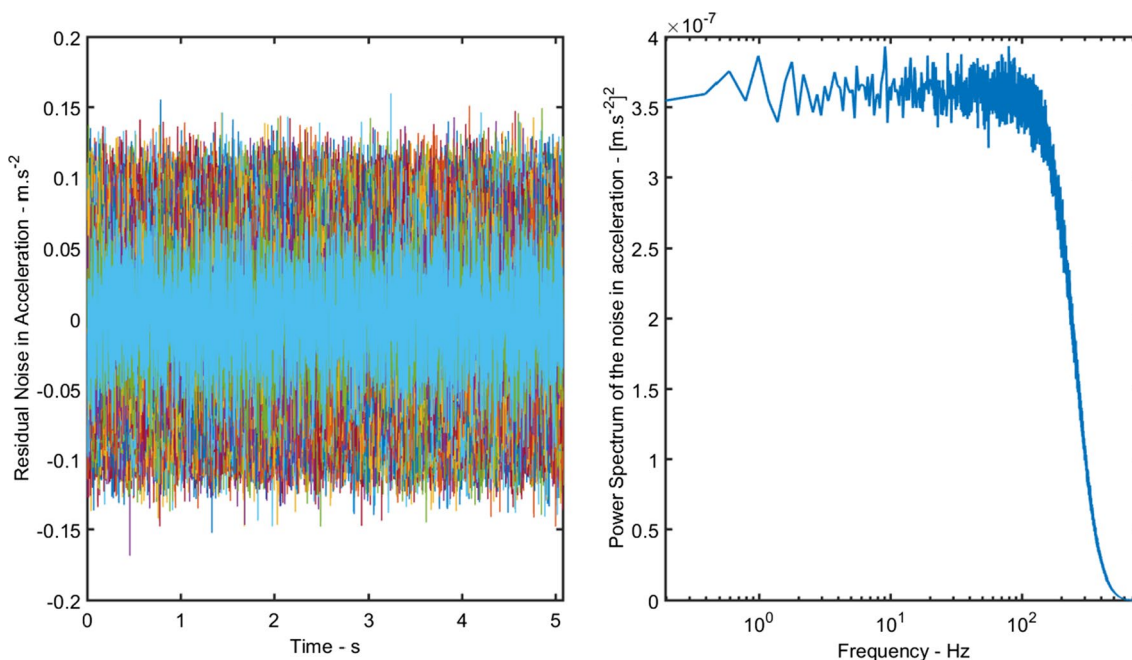


Fig. 1 Simulation of 1000 noise samples in an acceleration measurement system, using an acceleration noise density $N_d = 190 \mu g / \sqrt{\text{Hz}}$, filtered at $f_c = 250 \text{ Hz}$

frequency, Eq. (3) can be used to estimate the power spectrum of the low-frequency noise. For instance, in the power spectrum shown in Fig. 1, $P_{aa}(1) \approx 3.6 \cdot 10^{-7} \text{ m}^2 \cdot \text{s}^{-4}$, a value that agrees with Eq. (3), since $N_d = 190 \mu g / \sqrt{\text{Hz}}$.

2.2 Residual noise in the velocities calculated by numerically integrating acceleration signals

The mean value of the noise can be estimated from

$$\hat{\mu}_a = \frac{1}{N} \sum_{k=1}^N a(k). \tag{4}$$

Since the noise is a random process, its mean value has a Gaussian distribution centered at zero, and the variance of its estimation can be estimated using Eq. (5) [26].

$$\text{Var}[\hat{\mu}_a] \approx \frac{\sigma_a^2}{2BT}. \tag{5}$$

In Eq. (5), B is the bandwidth of the signal and T is its acquisition time. The random error of the estimate $\hat{\mu}_a$ has a standard deviation shown in Eq. (6).

$$\sigma[\hat{\mu}_a] \approx \frac{1}{\sqrt{2T}} \frac{\sigma_a}{\sqrt{B}}. \tag{6}$$

Therefore, there is a probability of about 95% that the estimate $\hat{\mu}_a$ falls within the interval [26]

$$[-2 \cdot \sigma[\hat{\mu}_a] \leq \hat{\mu}_a < 2 \cdot \sigma[\hat{\mu}_a]]. \tag{7}$$

The integration of this signal will result in a velocity signal that is a random walk with zero mean and values falling inside the interval shown in Eq. (8) [22].

$$\left[-\sqrt{2} \cdot \frac{\sigma_a}{\sqrt{B}} \cdot t^{1/2} \leq v^T(k) < \sqrt{2} \cdot \frac{\sigma_a}{\sqrt{B}} \cdot t^{1/2} \right]. \tag{8}$$

The double integration will result in a random walk signal with zero mean and values falling inside the interval shown in Eq. (9) [22].

$$\left[-\frac{\sqrt{2}}{2} \cdot \frac{\sigma_a}{\sqrt{B}} \cdot t^{3/2} \leq x^T(k) < \frac{\sqrt{2}}{2} \cdot \frac{\sigma_a}{\sqrt{B}} \cdot t^{3/2} \right]. \tag{9}$$

Figure 2 shows a typical result of this double integration using the extended trapezoidal rule [22].

The classic methods for double-integrating acceleration signals remove this random walk process, but the variance around zero persists. Since the objective is to analyze the effect of the noise in the resolution of the integration process, the mean value of each sample must be removed, as shown in Eq. (10), and the variance will be analyzed.

$$a_f(k) = a(k) - \frac{1}{N} \sum_{j=1}^N a(j) \quad k = 1, \dots, N. \tag{10}$$

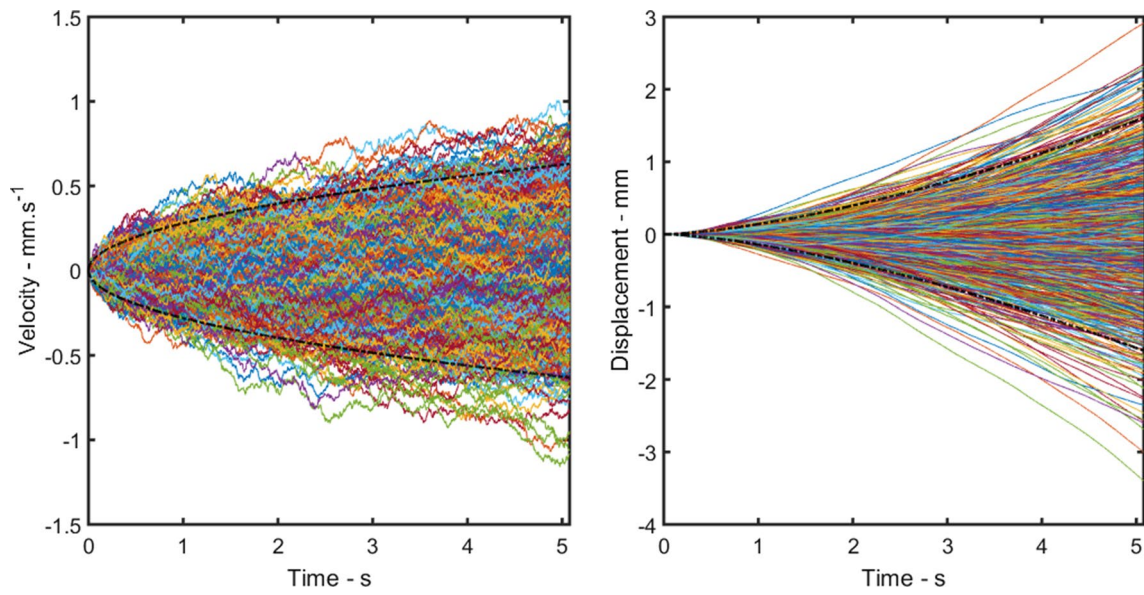


Fig. 2 Typical velocities and displacements obtained using the trapezoidal rule on white noise signals

The trapezoidal rule used to integrate Fig. 1 data sample is shown in Eq. (11), where $v^T(k)$ is the estimation of the actual value of $v(t)$ at every t_k time of the sample.

$$\begin{cases} v^T(1) = v_0 \\ v^T(k) = v^T(k-1) + \frac{\Delta t}{2} [a_f(k-1) + a_f(k)] \end{cases} \quad k = 2, \dots, N \quad (11)$$

For each sample, it is considered that $v_0 = 0$, but, since this is not necessarily true, the calculated velocity signal

must be corrected removing its mean value as shown in Eq. (12).

$$v_f^T(k) = v^T(k) - \frac{1}{N} \sum_{j=1}^N v^T(j) \quad k = 1, \dots, N. \quad (12)$$

Figure 3 shows the 1000 velocities samples resulting from the integration of Fig. 1 signals.

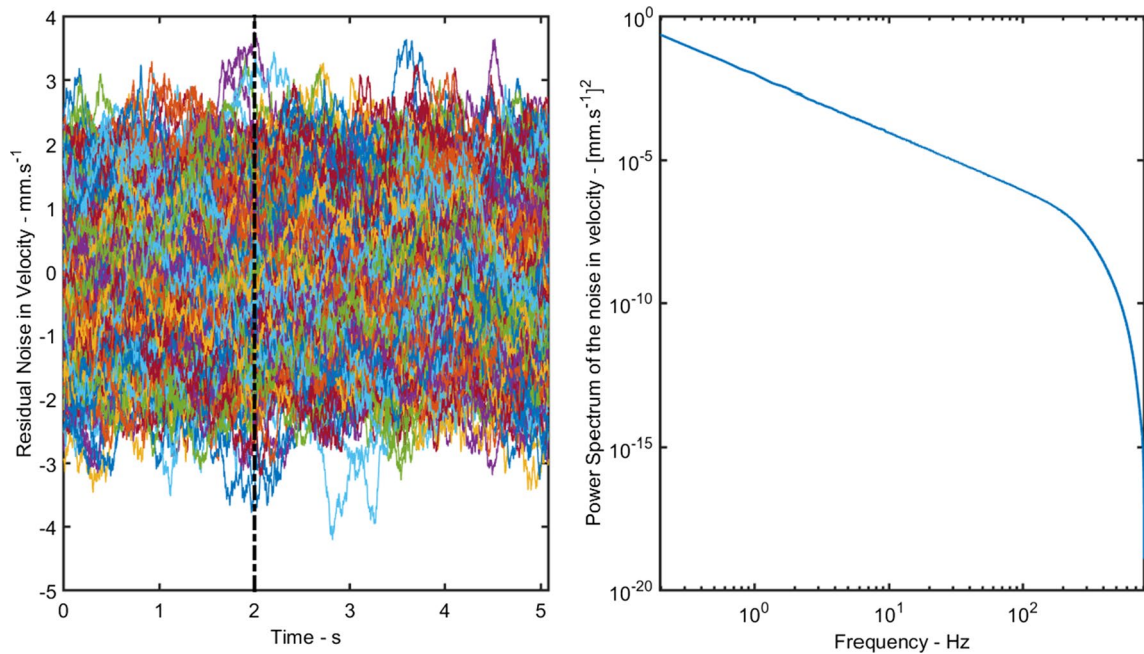


Fig. 3 Residual noise in the velocity obtained by integrating the 1000 samples shown in Fig. 1, and their mean power spectrum

Figure 4 shows the probability density function of only one of the samples shown in Fig. 3, which presents a non-Gaussian aspect, and the probability density function of all samples that presents a clear Gaussian aspect with a standard deviation of $\hat{\sigma}_v = 0.88 \text{ mms}^{-1}$.

For a non-ergodic signal, the variance can be calculated using the values of a specific instant of time of each sample.

Therefore, Fig. 5 shows the values of each velocity sample at an instant $t = 2s$, with its histogram depicted in blue and its theoretical probability density function $p(v_f^T)$ plotted in red, calculated using the estimated $\hat{\sigma}_v = 0.88 \text{ mms}^{-1}$. It can be concluded that the velocity signal is a non-ergodic random signal with zero mean value and normal distribution

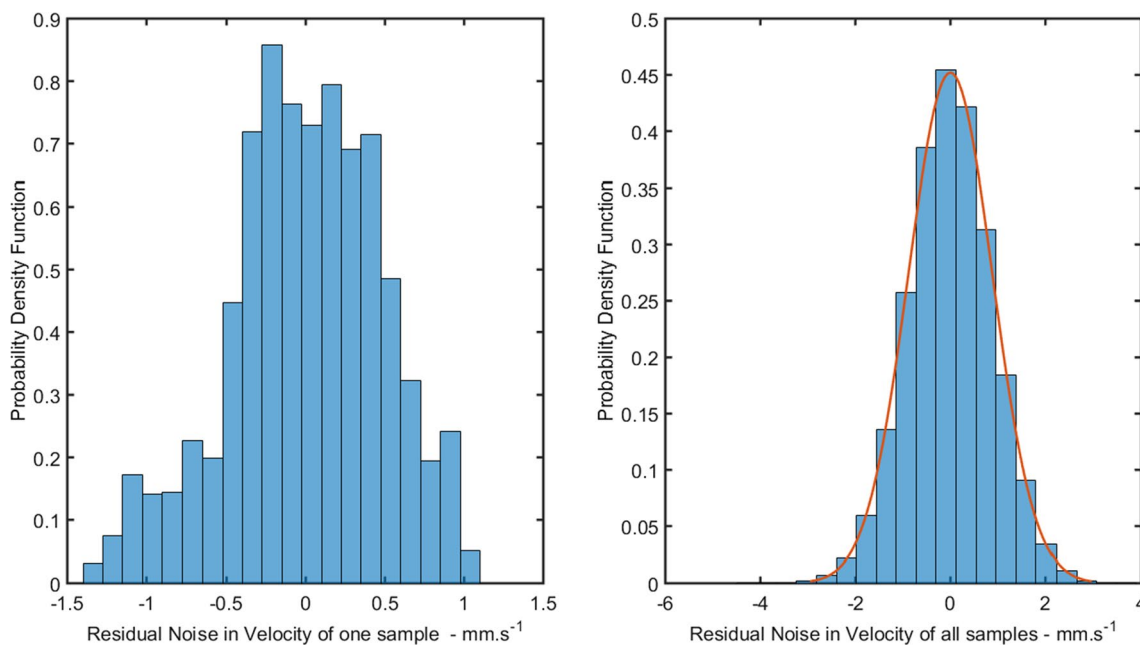


Fig. 4 Probability density functions of the velocity for one specific sample and for all 1000 samples

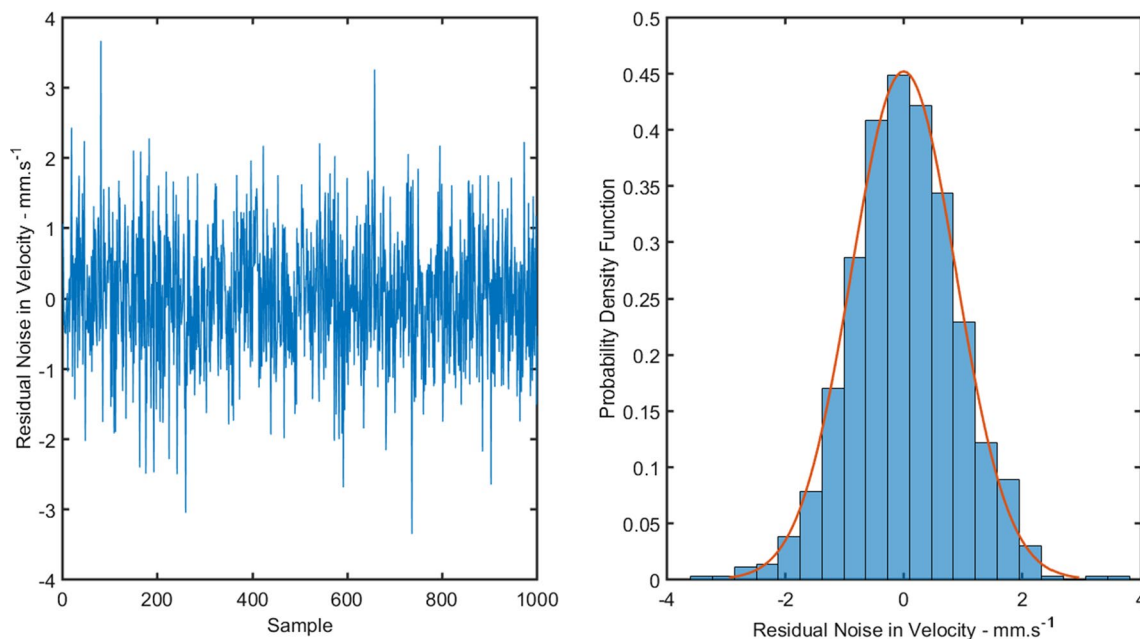


Fig. 5 Velocities at $t = 2s$ of each of the 1000 samples shown in Fig. 3

Table 1 Summary of the calculated velocity results, in mm/s

Measurement parameter	Statistics		
	Maximum	Minimum	Mean value
Peak	3.76	0.78	1.86
Valley	4.21	0.83	1.87
Peak-to-valley	7.12	1.65	3.73

described by Eq. (13) [26], where $p(v_f^T)$ is the probability density function of the velocity, obtained by integrating the acceleration noise.

$$p(v_f^T) = \frac{1}{\hat{\sigma}_v \sqrt{2\pi}} e^{-\frac{1}{2}(\frac{v_f^T}{\hat{\sigma}_v})^2} \tag{13}$$

This formula is valid for any sample time and can be particularly useful to estimate its peak velocity, since it is expected that 99.994% of these normally distributed values are between $\pm 4 \cdot \hat{\sigma}_v$. However, $\hat{\sigma}_v$ is time dependent and for this case with $T = 5.08s$, $\hat{\sigma}_v = 0.88 \text{ mm s}^{-1}$ and $\pm 4\hat{\sigma}_v = \pm 3.52 \text{ mm s}^{-1}$.

Table 1 lists some statistical parameters of Fig. 3 velocity signals, among them the maximum peak of the calculated velocities, which is coherent with the expected maximum of $\pm 4[\hat{\sigma}_v]$. Therefore, its expected standard deviation $\hat{\sigma}_v$ can be used as an estimator of the resolution obtainable from the integrated acceleration data.

Clearly, a formula for calculating $\hat{\sigma}_v$ based on the noise density of a sample time can be very useful, and it can be deduced using the power spectrum of the velocity P_{vv}^T combined with Parseval’s equation. However, since the noise density is related to P_{aa} , it is necessary to obtain the relation between them. This relation can be obtained using the Z-transform, since they are digital signals. From the definition of the extended trapezoidal rule, Eq. (14) can then be deduced.

$$V^T(z) - z^{-1}V^T(z) = \frac{\Delta t}{2} [A(z) - z^{-1}A(z)]. \tag{14}$$

After some algebraic manipulations and considering that $z = e^{j2\pi n/N}$, Eq. (15) is obtained.

$$V^T(n) = \frac{\Delta t}{2} \frac{1 + e^{-j2\pi \frac{n}{N}}}{1 - e^{-j2\pi \frac{n}{N}}} A(n) \quad n = 1, \dots, N - 1. \tag{15}$$

A transfer function $G_{vv}^T(n)$ between $(\Delta t/2) \cdot A(n)$ and $V^T(n)$ is defined, as shown in Eq. (16).

$$G_{vv}^T(n) = \frac{1 + e^{-j2\pi \frac{n}{N}}}{1 - e^{-j2\pi \frac{n}{N}}} \quad n = 1, \dots, N - 1. \tag{16}$$

This transfer function is not defined for $n = 0$ or for $n = N$, but this is not a problem since the DC component is not analyzed. Hence, the relation between the power spectra of the acceleration $P_{aa}(n)$ and of the calculated velocity $P_{vv}^T(n)$ for all nonzero frequency components is given by Eq. (17).

$$P_{vv}^T(n) = \left(\frac{\Delta t}{2}\right)^2 |G_{vv}^T(n)|^2 P_{aa}(n) \quad n = 1, \dots, N - 1. \tag{17}$$

Equation (17) can be used to estimate the variance $\hat{\sigma}_v^2$ of the velocity noise using Parseval’s equation once more, as depicted in Eq. (18).

$$\hat{\sigma}_v^2 = \sum_{n=1}^N P_{vv}^T(n) = \left(\frac{\Delta t}{2}\right)^2 P_{aa} \sum_{n=1}^N |G_{vv}^T(n)|^2. \tag{18}$$

A simple computational summation can verify that Eq. (19) is valid for large values of N , especially if $N \geq 128$. Since this is the case in acquisition of acceleration signals, this equation can be used for practical purposes.

$$\sum_{n=1}^{N-1} |G_{vv}^T(n)|^2 = 2 \sum_{n=1}^{N/2} |G_{vv}^T(n)|^2 \approx \frac{N^2}{3}. \tag{19}$$

Equation (18) is valid only if P_{aa} is constant for all frequencies, but this is not the case for the low-pass-filtered signal used. However, the validity of this approximation can be verified analyzing the influence of each frequency component in the $\hat{\sigma}_v$ value.

Table 2 shows the accumulation of Eq. (19) summations, and it demonstrates that the first 30 components are responsible for 98.04% of the resulting standard deviation and that Eq. (18) can be used, since the low-pass cutoff frequency is above that band. Therefore, the velocity resolution is not influenced by a low-pass filter with a cutoff frequency lower than the Nyquist frequency.

Then, using Eqs. (3), (18), and (19), the desired formula to estimate the standard deviation of the velocity noise is finally obtained in Eq. (20), where T is the total acquisition time.

Table 2 Effect of low frequencies in the velocity noise for N = 8192

n	$\left[2 \sum_{k=1}^n G_{vv}^T(k) ^2\right] \times 10^{-7}$	Accumulation %
1	1.36	60.82
2	1.70	76.02
3	1.85	82.78
4	1.94	86.57
30	2.19	98.04
4096	2.27	100.00

$$\hat{\sigma}_v \approx N_d \cdot \sqrt{T/24}. \tag{20}$$

Some important practical conclusions can be drawn from this numerical simulation exercise: the resolution of the velocities obtained by numerically integrating a (unavoidably) noisy acceleration signal is reduced by using a low-noise accelerometer and short sample times, and it is independent of the sample frequency.

2.3 Residual noise in the displacements obtained by double-integrating acceleration signals

After obtaining acceleration and velocity data, the resulting displacements can be estimated by numerically integrating the velocity signals using the extended trapezoidal rule once again, as shown in Eq. (21), where $x^T(k)$ is the estimation of the actual value of $x(t)$ at t_k .

$$\begin{cases} x^T(1) = x_0 \\ x^T(k) = x^T(k-1) + \frac{\Delta t}{2} [v_f^T(k-1) + v_f^T(k)] \end{cases} \quad k = 2, \dots, N \tag{21}$$

Figure 6 shows the simulation of 1000 displacements samples obtained by double-integrating the signals shown in Fig. 1, considering $v_0 = x_0 = 0$ and then removing its mean value, as shown in Eq. (22).

$$x_f^T(k) = x^T(k) - \frac{1}{N} \sum_{j=1}^N x^T(j) \quad k = 1, \dots, N. \tag{22}$$

Figure 6 shows the 1000 displacements samples resulting from the double integration of Fig. 1 signals.

Figure 7 shows the probability density function of only one of the samples shown in Fig. 6, which presents a non-Gaussian aspect, and the probability density function of all samples that presents a clear Gaussian aspect with a standard deviation of $\hat{\sigma}_x = 0.57\text{mm}$.

Figure 8 shows the values of each displacement sample at an instant $t = 2\text{s}$, with its histogram depicted in blue and its theoretical probability density function $p(x_f^T)$ plotted in red, calculated using a value of $\hat{\sigma}_x = 0.59\text{ mm}$ for its standard deviation.

Therefore, it is possible to conclude that the resulting signal is a non-ergodic random signal with zero mean value and a normal distribution expressed by Eq. (23).

$$p(x_f^T) = \frac{1}{\hat{\sigma}_x \sqrt{2\pi}} e^{-\frac{1}{2} \left(\frac{x_f^T}{\hat{\sigma}_x}\right)^2} \tag{23}$$

This formula is valid for any sample time and can be particularly useful to estimate the peak displacement, since it is expected that 99.994% of these normally distributed values are between $\pm 4 \cdot \hat{\sigma}_x$. But $\hat{\sigma}_x$ is time dependent and for this case with $T = 5.08\text{ s}$, $\hat{\sigma}_x = 0.57\text{ mm}$ and $\pm 4\hat{\sigma}_x = \pm 2.28\text{mm}$.

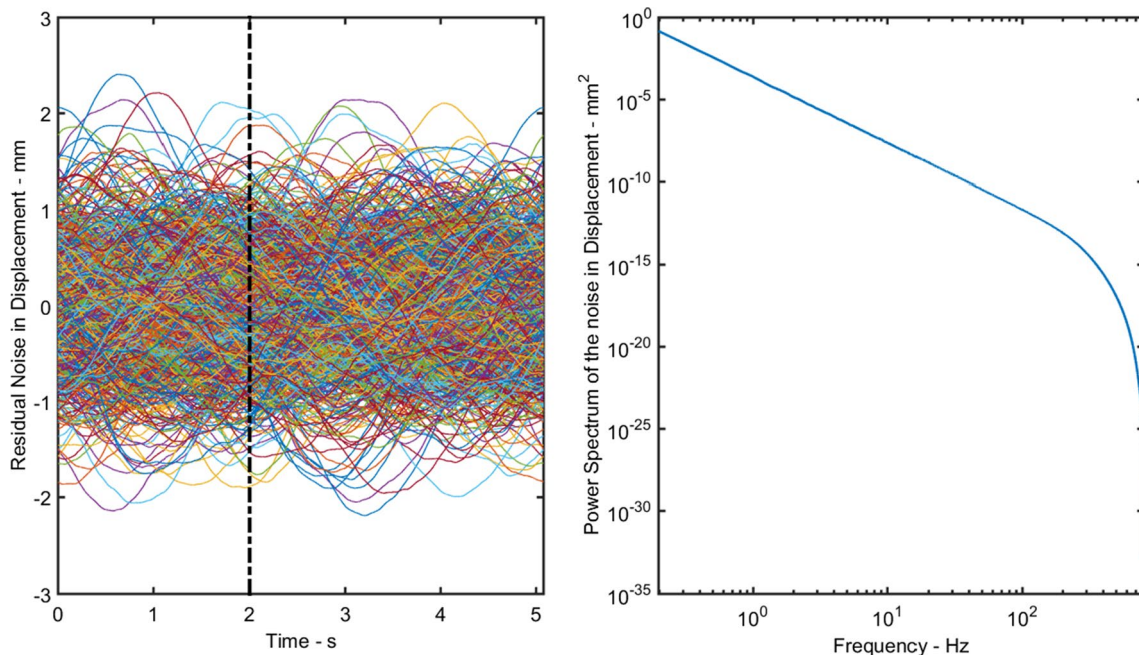


Fig. 6 Residual noise in the displacement obtained by numerically double-integrating the acceleration signals shown in Fig. 1 with a noise density $N_d = 190\mu\text{g}/\sqrt{\text{Hz}}$, filtered at $f_c = 250\text{ Hz}$ the 1000 samples shown in Fig. 1, and their mean power spectrum

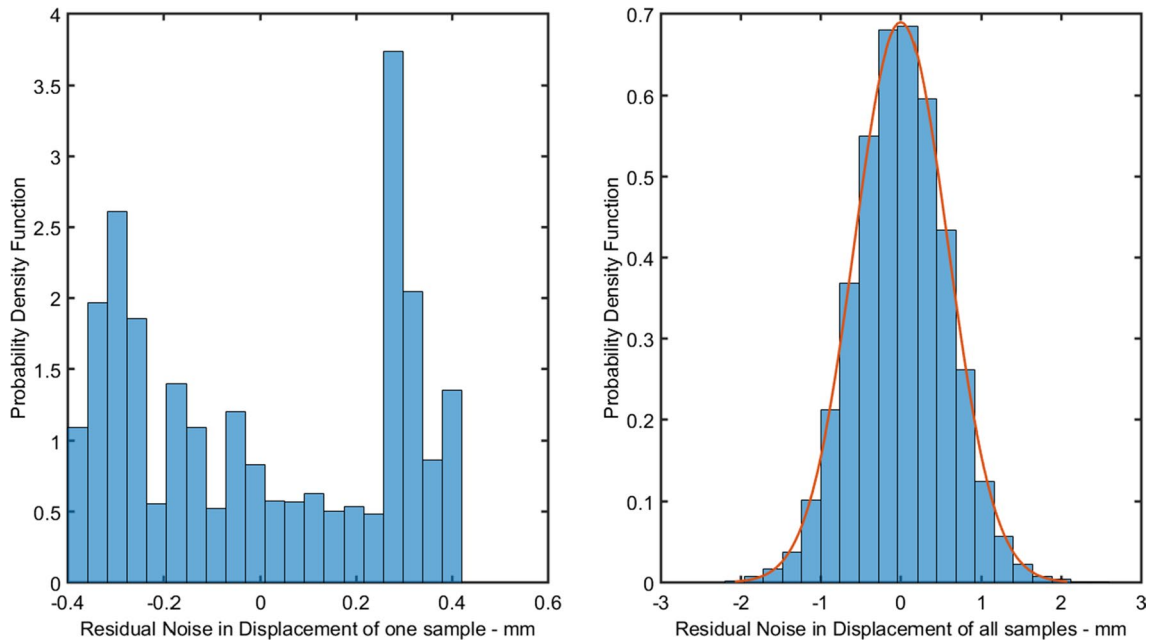


Fig. 7 Probability density functions of the displacement for one specific sample and for all 1000 samples

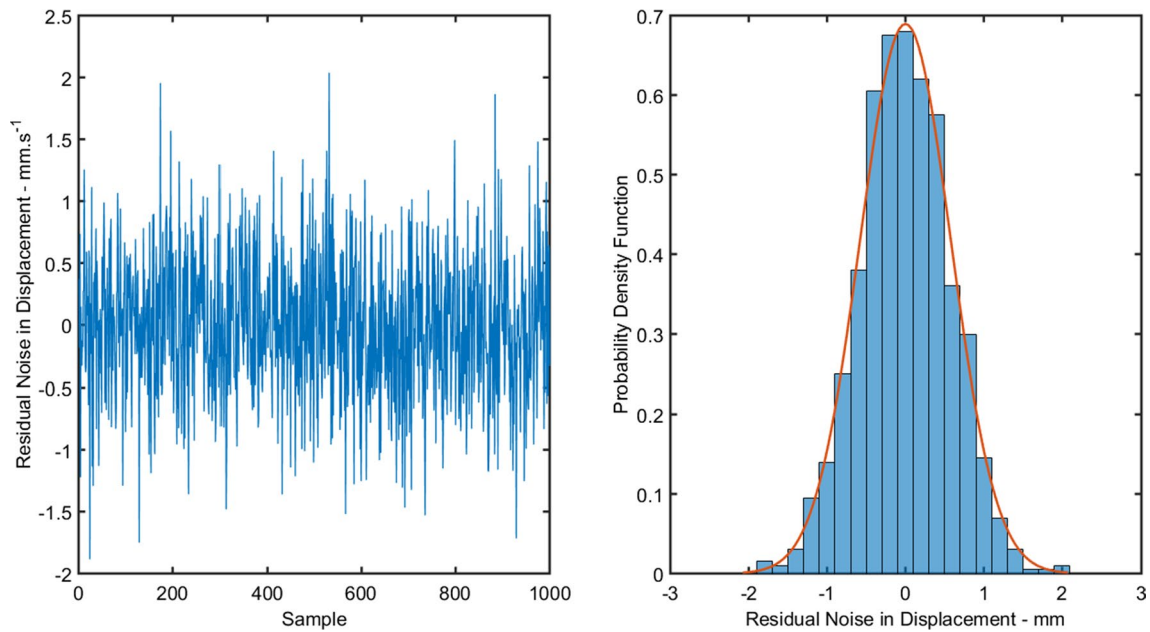


Fig. 8 Displacements at $t = 2s$ of each of the 1000 samples and its probability density

Table 3 shows some statistical parameters of the displacement signals shown in Fig. 6, such as the maximum peak of the calculated displacements, which is coherent with the expected maximum obtained within $\pm 4[\hat{\sigma}_x]$. Hence, a formula for calculating the expected standard deviation $\hat{\sigma}_x$ of the displacements can be used as an estimator of the resolution obtainable from the double integration of acceleration data.

Table 3 Summary of displacements results, in mm

Measurement parameter	Statistics		
	Maximum	Minimum	Mean value
Peak	2.41	0.16	0.80
Valley	2.19	0.12	0.80
Peak-to-valley	4.28	0.29	1.60

The procedure applied in the preceding section can be used once again to obtain Eq. (24), which shows the relation between $\hat{\sigma}_x$ and P_{aa} .

$$\begin{aligned} \hat{\sigma}_x^2 &= \sum_{n=1}^N P_{xx}^T(n) = \left(\frac{\Delta t}{2}\right)^4 \sum_{n=1}^N \left|G_{vv}^T(n)\right|^4 P_{aa}(n) \\ &= \left(\frac{\Delta t}{2}\right)^4 P_{aa} \sum_{n=1}^N \left|G_{vv}^T(n)\right|^4. \end{aligned} \tag{24}$$

A simple computational summation can verify that Eq. (25) is valid for large values of N , specially for $N \geq 128$. Since this is the case in acquisition of acceleration signals, this equation can be used for practical purposes.

$$\sum_{n=1}^N \left|G_{vv}^T(n)\right|^4 = 2 \sum_{n=1}^{N/2} \left|G_{vv}^T(n)\right|^4 \approx \frac{N^4}{45}. \tag{25}$$

An observation is necessary here concerning the validity of Eq. (24), since the acceleration signal is low-pass-filtered and then its P_{aa} is not constant for all frequencies. Table 4 shows the accumulation of Eq. (25) summations, and it demonstrates that the first 4 components are responsible for 99.67% of the resulting standard deviation $\hat{\sigma}_x$. Therefore, Eq. (24) converges much faster than Eq. (18), since it basically depends on its first five frequency components.

Finally, using Eqs. (3), (24), and (25), the desired formula to estimate the standard deviation of the displacement noise (resulting from the double numerical integration of a noisy acceleration signal) can be obtained, see Eq. (26).

$$\hat{\sigma}_x \approx N_d \cdot \sqrt{T^3/1440}. \tag{26}$$

The same conclusions obtained in the preceding section for the velocity signals are valid for the displacement signals as well. That is, the noise present in the displacement signal depends on the sample time, and it is in order of $T^{3/2}$, independent of the sample frequency and the integration method used. If it is necessary to attenuate this displacement noise avoiding a high-pass filter, it is then necessary

to use a shorter sample time and/or an accelerometer with a low noise density.

3 Numerical simulations

This section verifies the utility of Eq. (26) through numerical simulations of the double integration of a noisy acceleration signal. Figure 9 shows a displacement signal with 5 mm peak level and a frequency of 4.1 Hz, as well as its corresponding acceleration signal that has been corrupted by a noise with the characteristics shown in Fig. 1.

Figure 9 shows the double integration results of this noisy acceleration signal using the FFT-DDI method. For comparison purposes, Fig. 9 also shows the results obtained using a traditional technique called time domain trend removal (TDTR), which is the base of most numerical double integration methods [3–6]. The TDTR method is based on the adjustment of the acceleration, velocity, and displacements signals using the least square method, and can be combined with other processes, such as a high-pass filter [19–21].

According to Eq. (26), the double integration of this signal results in $\hat{\sigma}_x = 4.58 \text{ mm}$, hence the error in displacements can be as high as 18.34 mm. This can be verified in Table 5, which summarizes the results obtained from the FFT-DDI method. The lower error presented by the TDTR is due to the usage of the least square methods (Fig. 10).

Since the error introduced by the noise can be reduced using lower time integrations, it is worth to double-integrate this signal using piecewise integration with a time interval of $T = 5.079s$, dividing the total sample of $T = 20.316s$ in four samples, which are integrated separately. It reduces the expected error of the displacement to $4\hat{\sigma}_x = 2.28 \text{ mm}$, but introduces jumps between consecutive samples.

Figure 11 shows the result of the numerical double integration of this acceleration signal using the FFT-DDI and the TDTR. Table 6 summarizes the results and presents a maximum absolute error of 3.37 mm, which is coherent with the expected error. The error of the TDTR is reduced significantly, as expected by Eq. (26).

Figure 12 shows the results of the double integration using this interval, $T = 2.54s$, which has an expected error in displacement of $4\hat{\sigma}_x = 0.80 \text{ mm}$. Table 7 summarizes the results and presents a maximum absolute error of 1.13 mm for the FFT-DDI method and 0.56 mm for the TDTR.

When using the FFT-DDI method detailed by Ribeiro et al. in [22], this minimum possible data acquisition interval is dependent on the minimum signal frequency f_{min} present in the acceleration signal, as shown in Eq. (27).

$$T_{min} = 5/f_{min} \tag{27}$$

Table 4 Effect of the low frequencies in the displacement noise for $N = 8192$

n	$\left[2 \sum_{k=1}^n \left G_{vv}^T(k)\right ^4\right] \times 10^{-13}$	Accumulation %
1	9.25	92.40
2	9.82	98.17
3	9.94	99.31
4	9.98	99.67
5	9.99	99.82
4096	10.01	100.00

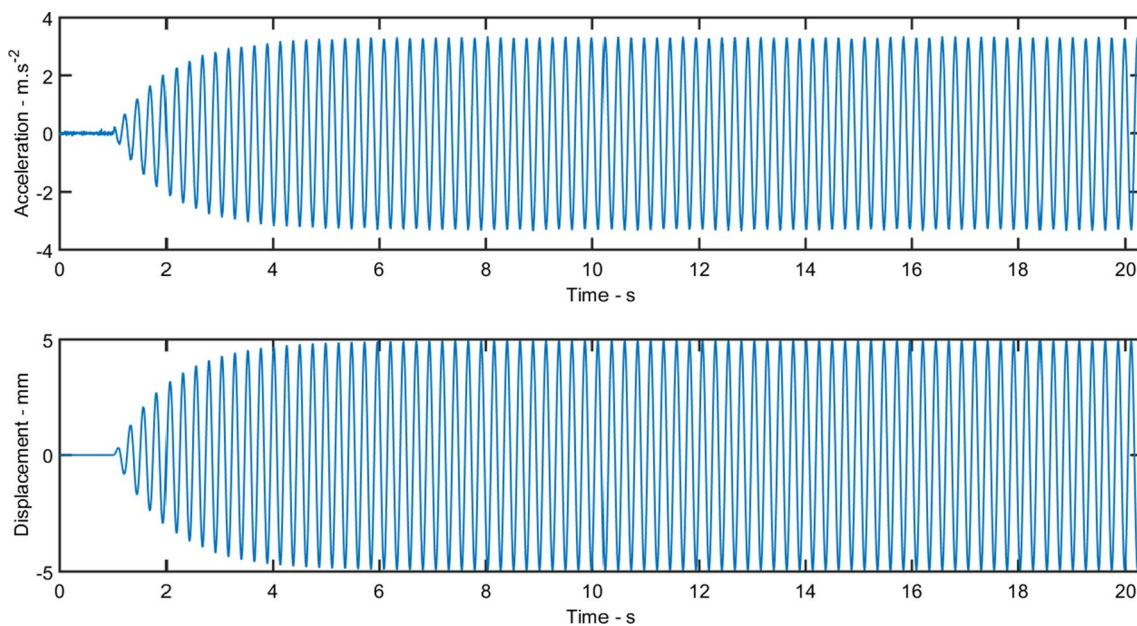


Fig. 9 Displacements and corresponding noisy acceleration generated from numerical simulations

Table 5 Summary of the results shown in Fig. 10

Parameter	Actual (mm)	FFT-DDI			TDTR		
		Calculated	Error		Calculated	Error	
			mm	%		mm	%
Peak	4.95	22.14	17.19	347.27	8.08	3.14	63.43
Valley	-4.95	-6.97	-2.02	40.91	-8.25	-3.30	66.78
Peak-to-valley	9.89	29.11	19.22	194.21	16.34	6.44	65.11

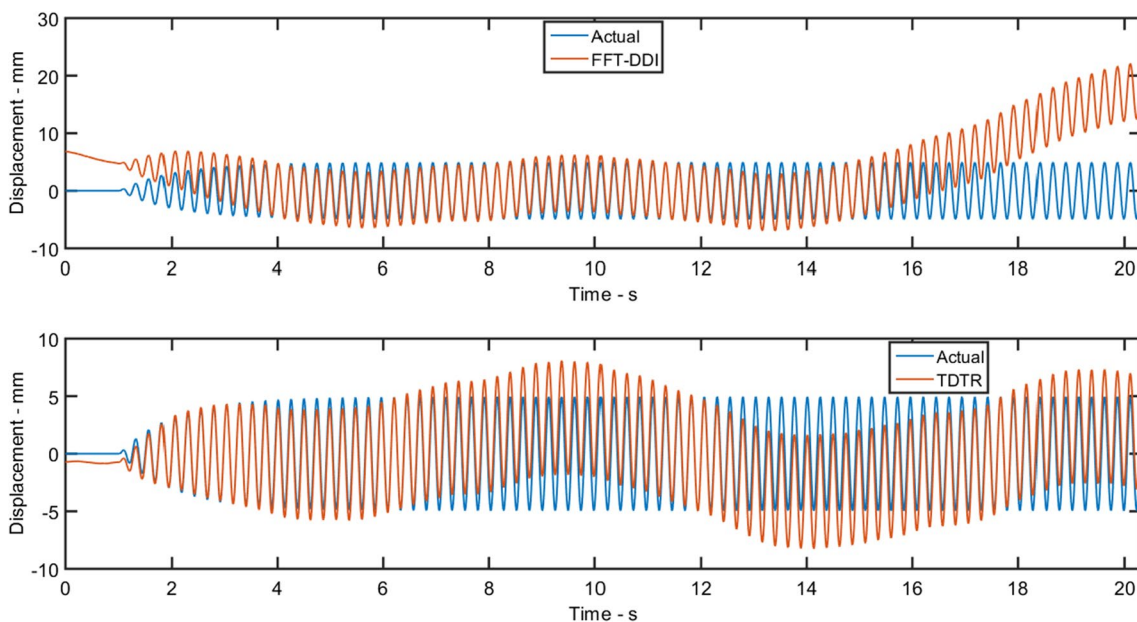


Fig. 10 Double integration of the noisy acceleration signal shown in Fig. 9 using the FFT-DDI method and the TDTR

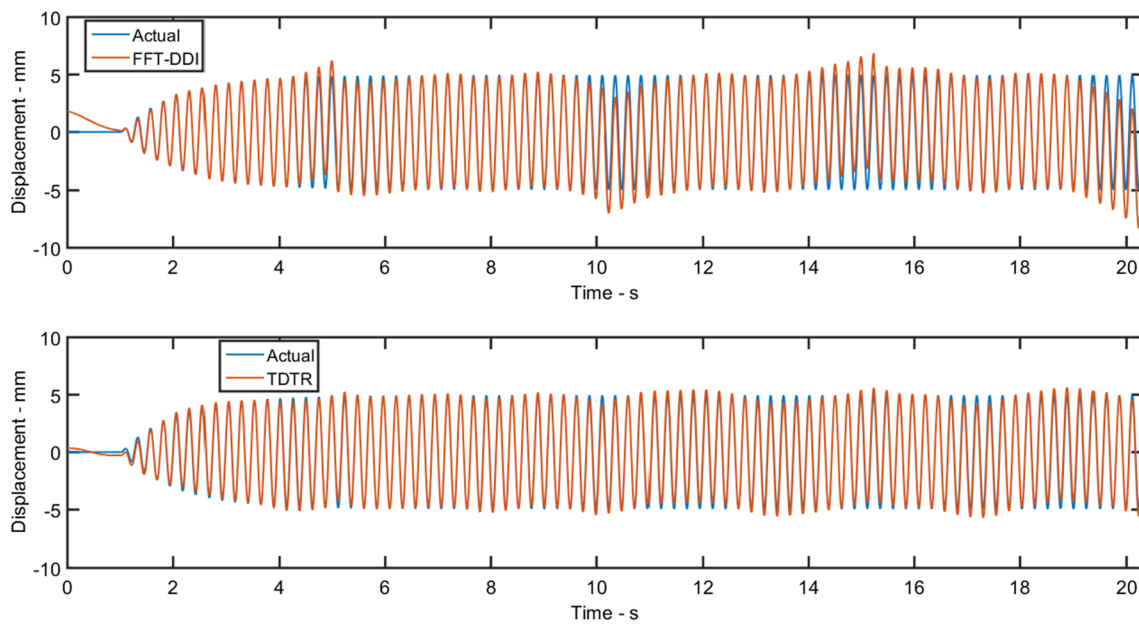


Fig. 11 Double integration of the noisy acceleration signal shown in Fig. 9 using the FFT-DDI method and the TDTR using a time interval of $T=5.079$ s

Table 6 Summary of the results shown in Fig. 11

Parameter	Actual (mm)	FFT-DDI			TDTR		
		Calculated	Error		Calculated	Error	
			mm	%		mm	%
Peak	4.95	6.85	1.91	38.61	5.63	0.69	13.84
Valley	-4.95	-8.32	-3.37	68.16	-5.70	-0.76	15.31
Peak-to-valley	9.89	15.18	5.28	53.39	11.33	1.44	14.58

Table 7 Summary of the results shown in Fig. 22

Parameter	Actual (mm)	FFT-DDI			TDTR		
		Calculated	Error		Calculated	Error	
			mm	%		mm	%
Peak	4.95	6.08	1.13	22.86	5.50	0.56	11.24
Valley	-4.95	-5.28	-0.33	6.74	-5.59	-0.65	13.08
Peak-to-valley	9.89	11.36	1.47	14.80	11.10	1.20	12.15

Since this signal frequency is $f = 4.1\text{Hz}$, the integration interval can be reduced to $T = 1.27\text{s}$ and then expected standard deviation is reduced to $\hat{\sigma}_x = 0.07\text{ mm}$ according to Eq. (26), so that 99.994% of the displacement noise is in the range $\pm 0.28\text{ mm}$. This result is shown in Fig. 12. Table 8 summarizes the results and presents a maximum absolute error of 0.21 mm for the FFT-DDI method and 0.69 mm for the TDTR. The error of the TDTR remains at 14%.

The most important conclusion at this point is that, by reducing the sample time, the error is reduced in both

methods. But the reduction of the TDTR is limited to about 14%, since least square method used depends on larger sample times. Therefore, for larger reductions, it depends on a high-pass filter. However, the FFT-DDI does not have this limitation, and thus, it can get a smaller error of about 4%.

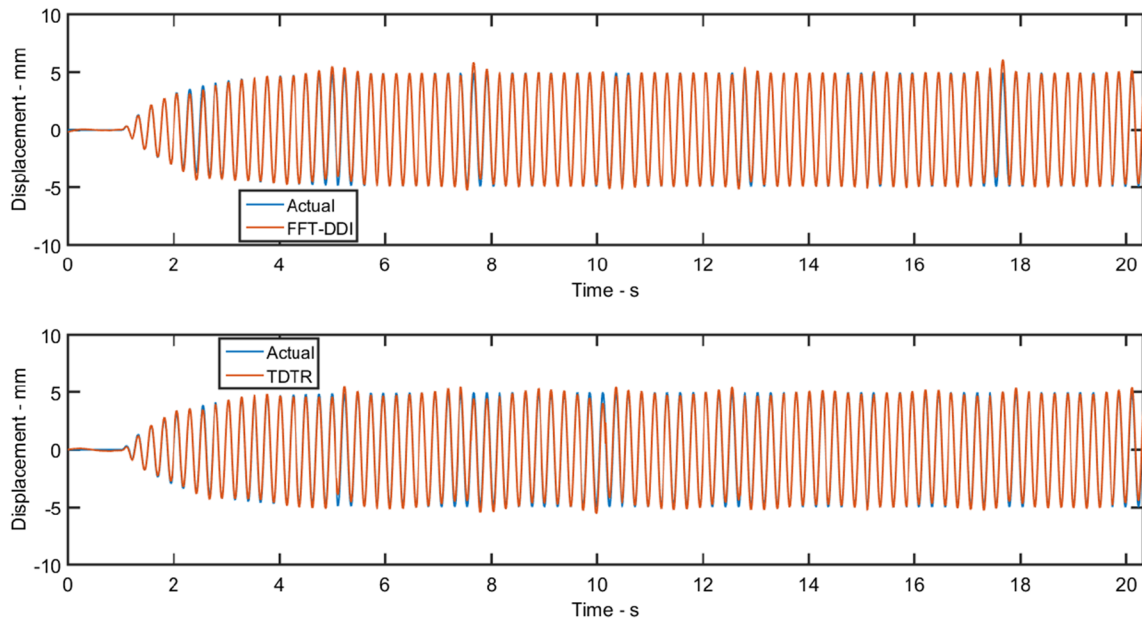


Fig. 12 Double integration of the noisy acceleration signal shown in Fig. 9 using the FFT-DDI method and the TDTR using a time interval of $T=2.54$ s

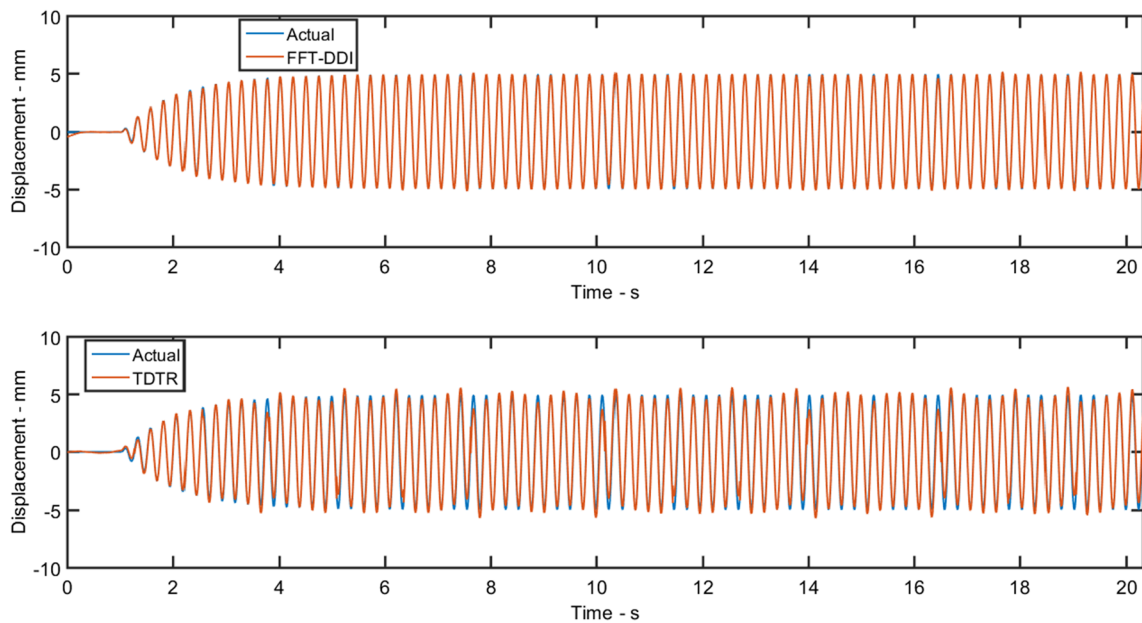


Fig. 13 Double integration of the noisy acceleration signal shown in Fig. 9 using the FFT-DDI method and the TDTR using a time interval of $T=1.27$ s

4 Experimental validation

The next step is to validate Eq. (26) experimentally, using a resistive accelerometer model AS-1 GB from Kyowa Electronic Instruments, connected to a signal conditioner model NI 9237 from National Instruments, measuring

displacements using the FFT-DDI and the TDTR techniques. This accelerometer sensor is chosen because it is based on strain gauge sensors; therefore, it is sensitive to static acceleration components. The acquisition system is connected to a desktop using Windows 10 and Labview 2014.

The displacements have been generated in an Instron 8501 servohydraulic testing machine equipped with a LVDT

Table 8 Summary of the results shown in Fig. 12

Parameter	Actual (mm)	FFT-DDI			TDTR		
		Calculated	Error		Calculated	Error	
			mm	%		mm	%
Peak	4.95	5.16	0.21	4.21	5.64	0.69	13.92
Valley	-4.95	-5.14	-0.20	4.03	-5.68	-0.73	14.83
Peak-to-valley	9.89	10.30	0.41	4.12	11.32	1.42	14.38

transducer, which can be used to acquire directly the reference displacement signals, without any need to numerically treating them. The Kyowa accelerometer was mounted directly on the head of the hydraulic machine jack. Figure 13 shows the system used in such tests.

Figure 14 shows ten measurement samples with no dynamic acceleration, made to evaluate their noise level, as well as their power spectrum. This acceleration measurement system has an intrinsic noise standard deviation $\sigma_a = 55 \text{ mm/s}^2$. Its power spectrum is not flat, but since its low-frequency components are the main responsible for \hat{x} , the noise density can be estimated using the values of $P_{aa}(1)$ in Eq. (3), leading to an effective noise density $N_d = 55.2 \text{ } \mu\text{g}/\sqrt{\text{Hz}}$, since this value is not provided by the accelerometer manufacturer.

Figure 15 shows a sinusoidal displacement signal with 2 mm amplitude and frequency 4.1 Hz. The displacements are acquired from the LVDT, and the acceleration from the accelerometer. The acquisition sampling time has been set as $\Delta t = 0.00062\text{s}$.

Figure 16 shows the displacements calculated from the double integration of the acceleration signal using a time interval of $T = 20.32\text{s}$, resulting in $\hat{\sigma}_x = 1.33 \text{ mm}$. Table 9 summarizes the results and presents a maximum absolute error of 4.42 mm for the FFT-DDI method and 3.89 mm for the TDTR.

Figure 17 shows displacements resulting from the double integration with piecewise integration at time intervals $T = 5.079\text{s}$, resulting in $\hat{\sigma}_x = 0.17 \text{ mm}$. Table 10 summarizes the results and presents a maximum absolute error of

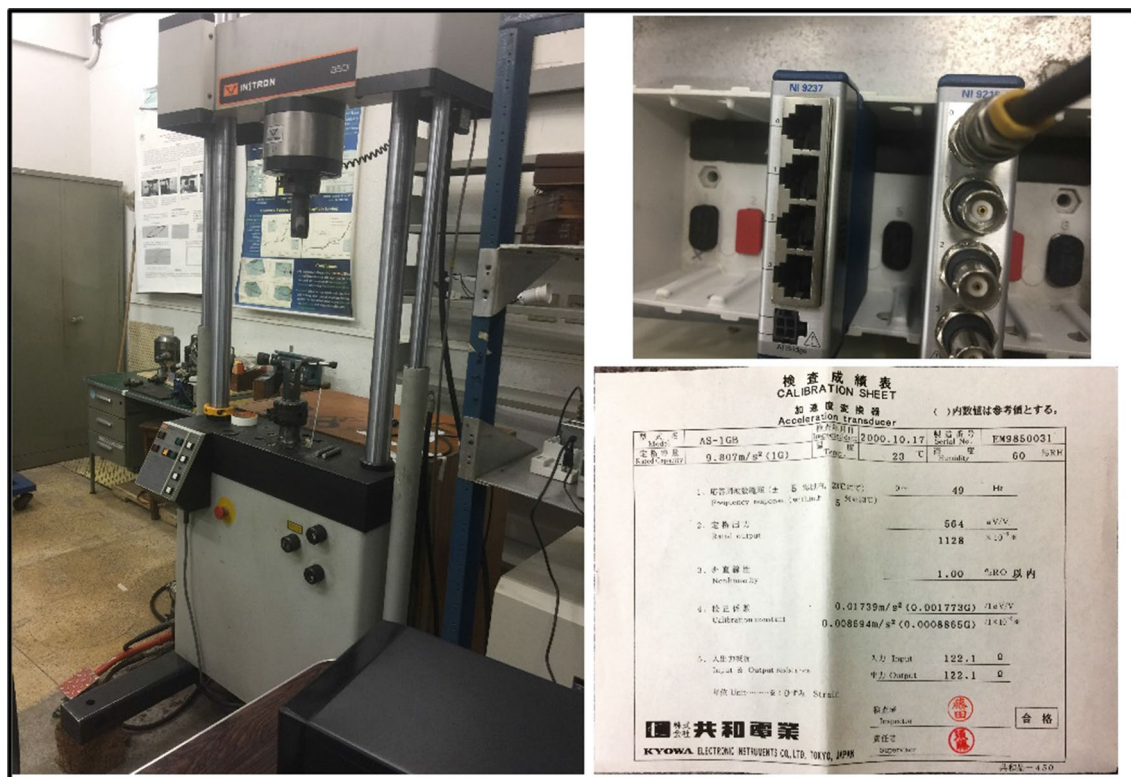


Fig. 14 System used to generate the displacements and to acquire the acceleration signals

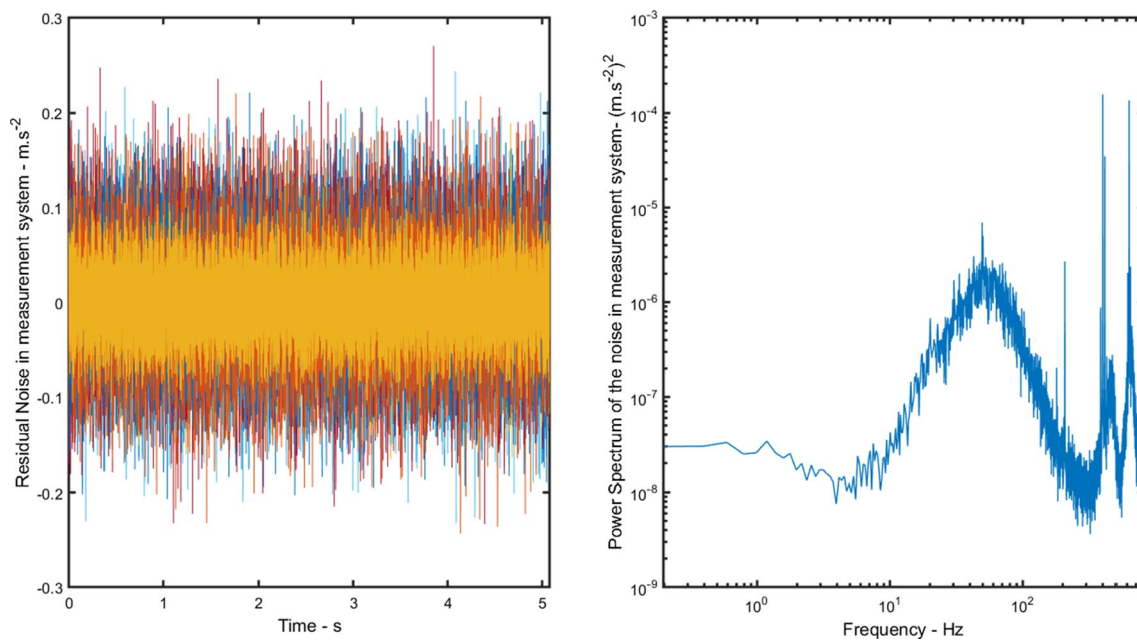


Fig. 15 Ten samples of the noise level measured in the acceleration measurement system

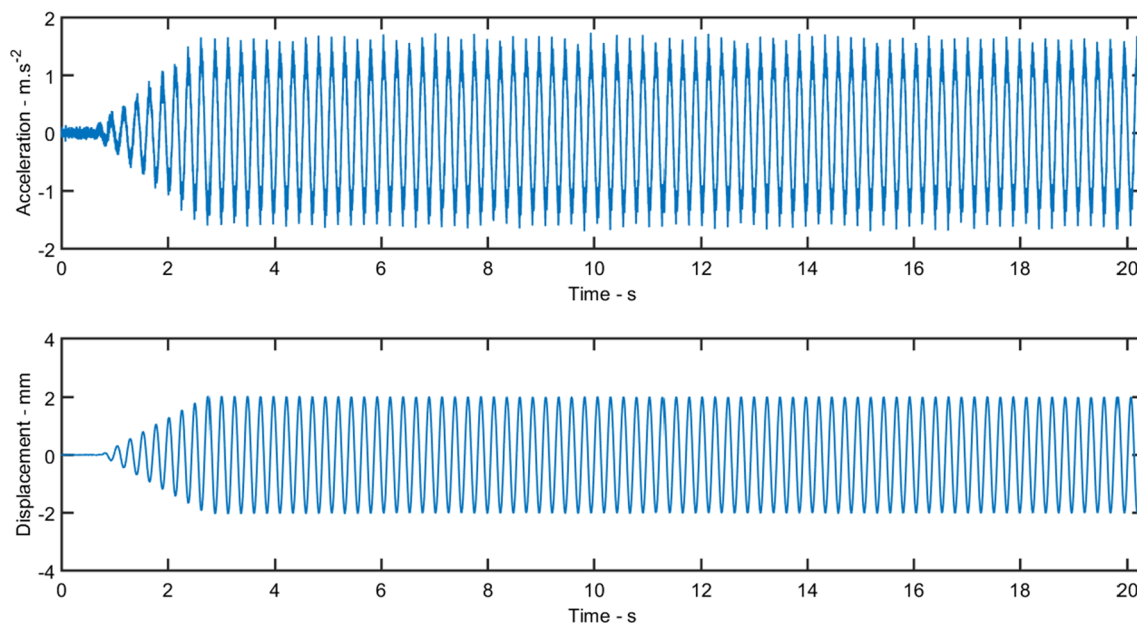


Fig. 16 Displacement of 2 mm and 4.1 Hz signal and the corresponding measured acceleration

−2.73 mm for the FFT-DDI method and 1.09 mm for the TDTR.

Figure 18 shows results of the double integration with piecewise integration at time intervals $T = 2.54s$, resulting in $\hat{\sigma}_x = 0.06 \text{ mm}$. Table 11 summarizes the results and presents a maximum absolute error of 0.31 mm for the FFT-DDI method and 0.22 mm for the TDTR.

Figure 19 shows results of the double integration with piecewise integration with time interval $T = 1.27s$, resulting in $\hat{\sigma}_x = 0.02 \text{ mm}$. Table 12 summarizes the results and presents a maximum absolute error of 0.04 mm for the FFT-DDI method and 0.25 mm for the TDTR.

Figure 20 shows a sinusoidal displacement signal with 2 mm amplitude and frequency 1.1 Hz. Since this frequency is low, the lowest time interval possible is $T = 5.079s$.

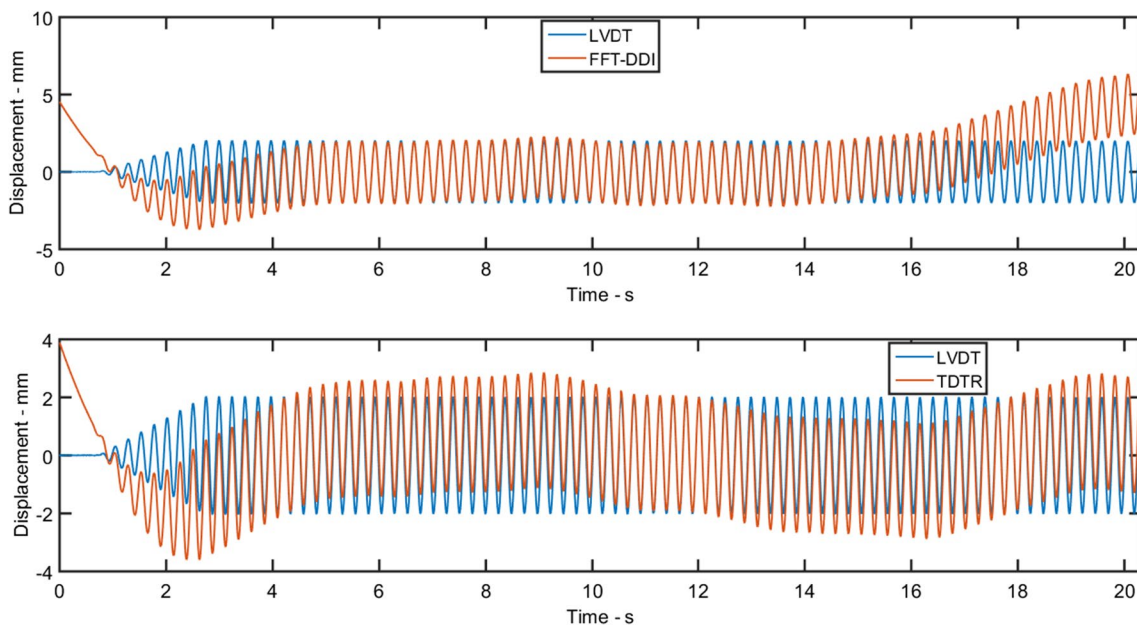


Fig. 17 Double integration of the noisy acceleration signal shown in Fig. 15 using the FFT-DDI method and the TDTR

Table 9 Summary of Fig. 17 results

Parameter	LVDT (mm)	FFT-DDI				TDTR			
		Calculated	Error		Calculated	Error			
			mm	%		mm	%		
Peak	2.04	6.46	4.42	216.98	3.89	1.85	90.93		
Valley	-2.04	-3.75	-1.71	83.59	-3.60	-1.56	76.53		
Peak-to-valley	4.08	10.21	6.13	150.22	7.50	3.41	83.72		

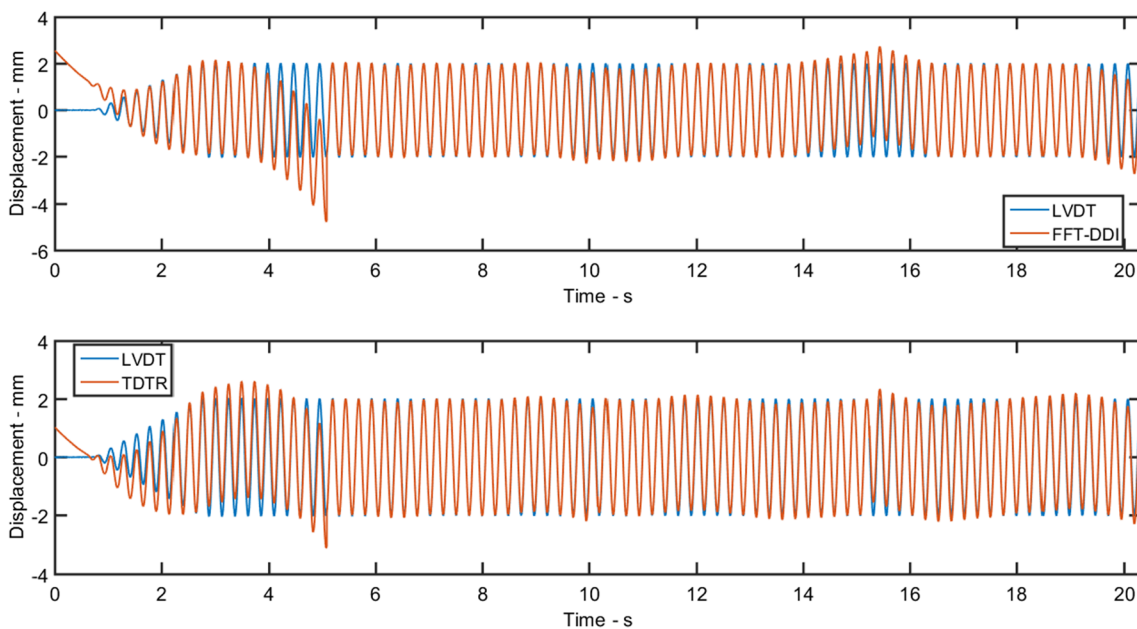


Fig. 18 Double integration of the noisy acceleration signal shown in Fig. 15 using the FFT-DDI method and the TDTR using a time interval of $T=5.079$ s

Table 10 Summary of Fig. 17 results

Parameter	LVDT (mm)	FFT-DDI			TDTR		
		Calculated	Error		Calculated	Error	
			mm	%		mm	%
Peak	2.04	2.74	0.71	34.67	2.62	0.58	28.54
Valley	-2.04	-4.78	-2.73	133.86	-3.13	-1.09	53.32
Peak-to-valley	4.08	7.52	3.44	84.31	5.75	1.67	40.94

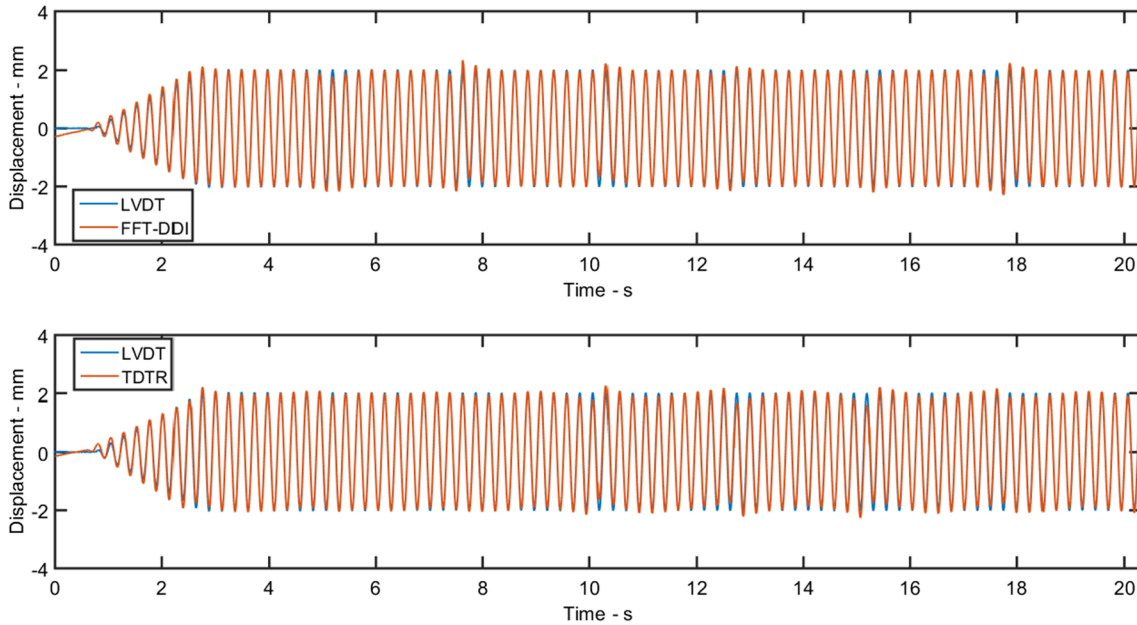


Fig. 19 Double integration of the noisy acceleration signal shown in Fig. 15 using the FFT-DDI method and the TDTR using a time interval of $T=2.54$ s

Table 11 Summary of Fig. 18 results

Parameter	LVDT (mm)	FFT-DDI			TDTR		
		Calculated	Error		Calculated	Error	
			mm	%		mm	%
Peak	2.04	2.34	0.31	15.00	2.25	0.22	10.63
Valley	-2.04	-2.30	-0.26	12.50	-2.26	-0.22	10.72
Peak-to-valley	4.08	4.64	0.56	13.75	4.52	0.44	10.68

Figure 21 shows results of the double integration with piecewise integration with time interval $T = 5.079s$, resulting in $\hat{\sigma}_x = 0.17mm$. Table 13 summarizes the results and presents a maximum absolute error of -1.30 mm for the FFT-DDI method and of -0.39 mm for the TDTR.

The results shown above validate Eq. (26) as a reference for estimating the expected error in the measurement of displacements using the double integration of acceleration signal.

5 Steps to minimize displacement errors in FFT-DDI algorithm

This section presents the procedures implemented in the algorithm used in this work to measure displacements by numerically double-integrating noisy acceleration signals. First, it is necessary to know the noise density of the measurement system. If it is not known, these three steps must be followed to estimate it:

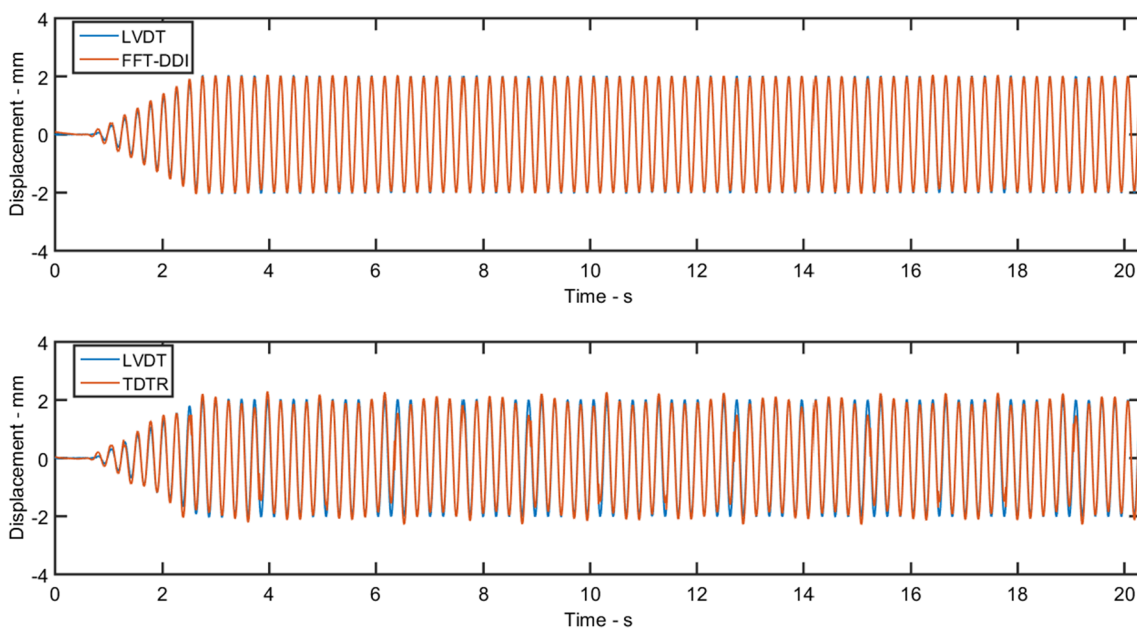


Fig. 20 Double integration of the noisy acceleration signal shown in Fig. 15 using the FFT-DDI method and the TDTR using a time interval of $T = 1.27$ s

Table 12 Summary of Fig. 19 results

Parameter	LVDT (mm)	FFT-DDI			TDTR		
		Calculated	Error		Calculated	Error	
			mm	%		mm	%
Peak	2.04	2.08	0.04	1.81	2.29	0.25	12.38
Valley	-2.04	-2.05	-0.01	0.30	-2.29	-0.24	11.99
Peak-to-valley	4.08	4.12	0.04	1.06	4.58	0.49	12.18

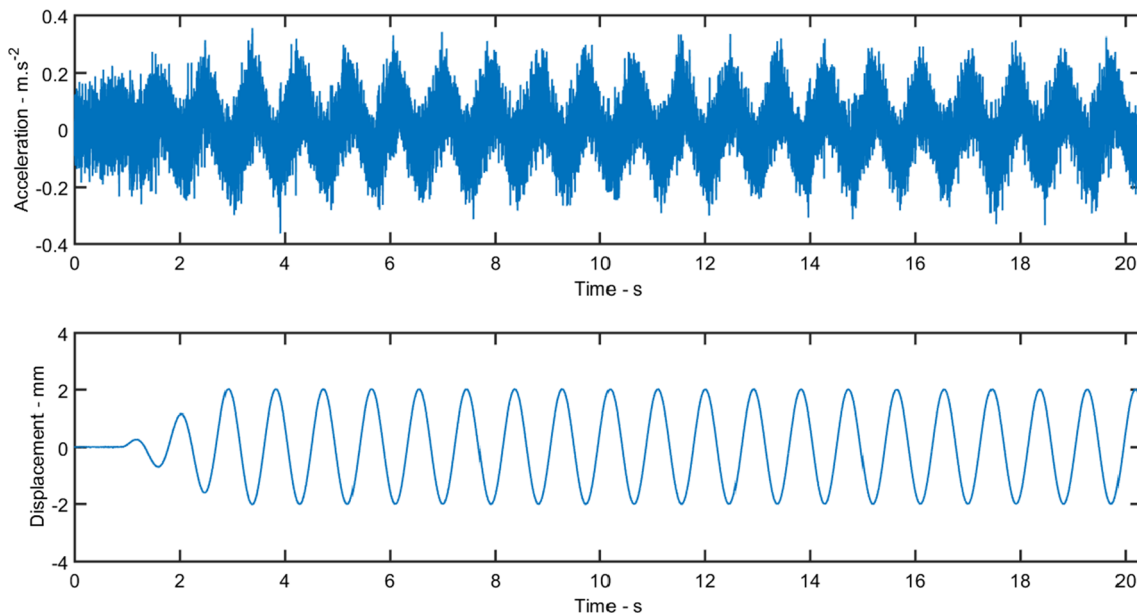


Fig. 21 Displacements with 2 mm amplitude at 1.1 Hz and corresponding measured accelerations

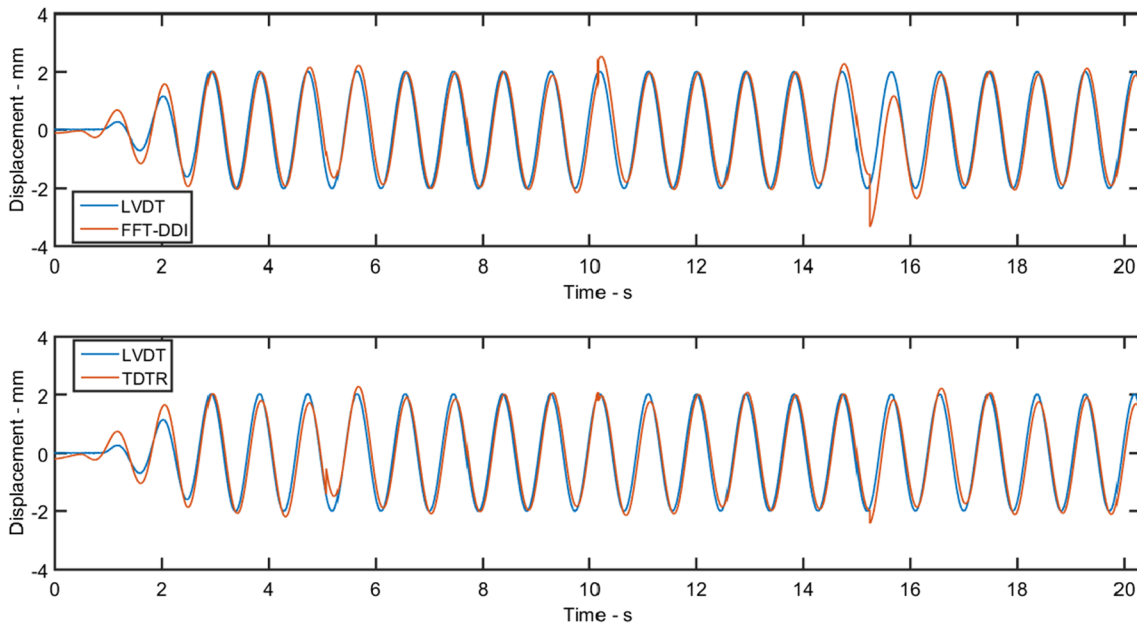


Fig. 22 Double integration of the noisy acceleration signal shown in Fig. 20 using the FFT-DDI method and the TDTR using a time interval of $T=5.079$ s

Table 13 Summary of Fig. 21 results

Parameter	LVDT (mm)	FFT-DDI			TDTR		
		Calculated	Error		Calculated	Error	
			mm	%		mm	%
Peak	2.04	2.53	0.49	24.04	2.28	0.23	11.48
Valley	-2.04	-3.33	-1.30	63.67	-2.43	-0.39	19.39
Peak-to-valley	4.08	5.87	1.79	43.82	4.71	0.63	15.43

- Acquire at least 10 samples of the signal from the acceleration measurement system, when in stationary state, to extract its noise.
- Calculate the power spectrum of the noise.
- With Eq. (3), estimate the noise density N_d of the system using the mean value of low-frequency components of P_{aa} .

Then, the integration algorithm follows a sequence of six steps:

- Acquire and digitize the acceleration signal with a convenient sample frequency.
- Using Eq. (27) with the minimum frequency of the signal, calculate the minimum necessary sample time to double-integrate the signal correctly, when using the FFT-DDI method.
- Divide the acceleration signal in segments with a sample time equal to the time calculated above.

- Double-integrate each one of the segments using the FFT-DDI algorithm, as detailed in Appendix 2.
- Calculate the expected error $\hat{\sigma}_x$ calculated using Eq. (26).
- Compare the calculated peak values and $\hat{\sigma}_x$. The lower $\hat{\sigma}_x$, the better the results.

The TDTR presents an ambiguous behavior. The value of $\hat{\sigma}_x$ can be reduced using lower sample time, but lower sample time increases the error of the TDTR method. In the FFT-DDI method, the sample time can be reduced to $5 \times$ the lowest period of the signal to reduce the effect the noise. This a good reason to choose the FFT-DDI method.

Figure 12 and Table 8 present the result of a simulation of the FFT-DDI method. In that situation, $\hat{\sigma}_x$ is 1.4% of the peak level and the peak error was 4.21%.

Figure 19 and Table 12 present an experimental result of the FFT-DDI method. In that situation, $\hat{\sigma}_x$ is 1% of the peak level and the peak error was 2%.

Therefore, it can be concluded that the FFT-DDI method can be used with a maximum permissible value for $\hat{\sigma}_x$ equal to 2% of the expected peak value to achieve an expected error of 4% in peak level. If it is not possible, the solution is to use an accelerometer with lower noise density.

Finally, it is worth to mention that, even if the signals used in this paper have only one frequency component, the FFT-DDI method can be used in any periodic and transient signals, even when a DC component is present. It can be used for quasi-periodic signals too, if the first frequency component is known. However, if the signal is random it can be more problematic, because it can have many very low-frequency components.

6 Conclusions

The main objective of this work was to formulate an algorithm to correctly measure displacements using noisy acceleration data, avoiding the need for a FIR high-pass filter and its limitations. A general formula has been introduced, properly estimating the error introduced by acceleration noise in calculated velocities and displacements. It has been validated through both simulations and experimental results. The resulting algorithm successfully provides improved displacement estimates in the presence of noise, with several practical applications.

Appendix 1: Used noise generator algorithm in Matlab

```
% The objective of this program is generating a gaussian noise with a desired
% noise density Nd and frequency band B
clear all;
%
% Definition of the parameters of the signal
Nt=1000;
N=8192;
dt=0.00062;
%
% Definition of the desired noise density of the
Nd=190;% Nd in micro g / square Hz
sa=Nd*sqrt(1/(2*dt))*1e-6;
%
% Definition of the desired low-pass filters
f1c=700;
f2c=500;
f3c=250;
f4c=100;
[bf1,af1]=butter(2,f1c/(1/dt/2));
[bf2,af2]=butter(2,f2c/(1/dt/2));
[bf3,af3]=butter(2,f3c/(1/dt/2));
[bf4,af4]=butter(2,f4c/(1/dt/2));
%
% Gaussian noise generation
ar=9*sa*wgn(1,N*(Nt+1),1);
a=ar(N+1:N*(Nt+1));
%
% Filtering of the acceleration
ap=filter(bf1,af1,ar);
a1=ap(N+1:N*(Nt+1));
ap=filter(bf2,af2,ar);
a2=ap(N+1:N*(Nt+1));
ap=filter(bf3,af3,ar);
a3=ap(N+1:N*(Nt+1));
ap=filter(bf4,af4,ar);
a4=ap(N+1:N*(Nt+1));
%
Nd=std(a)*sqrt(2*dt)*1e5;
% clear bf1 bf2 bf3 bf4 af1 af2 af3 af4 ar ap
```

Appendix 2: Proposed FFT-DDI algorithm in Matlab

```

%
% Matlab function for double integration of acceleration signal using the
% FFT_DDI method
%
function [v,x]=FFT_DDI(a,t)
%
v=zeros(1,length(a));
x=zeros(1,length(a));
%----- Filtering of the acceleration -----
A=fft(a);
da=(A(1)-det([(-3)^5 (-3)^4 (-3)^3 (-3)^2 (-3)^1 real(A(4));
(-2)^5 (-2)^4 (-2)^3 (-2)^2 (-2)^1 real(A(3));
(-1)^5 (-1)^4 (-1)^3 (-1)^2 (-1)^1 real(A(2));
(3)^5 (3)^4 (3)^3 (3)^2 (3)^1 real(A(4));
(2)^5 (2)^4 (2)^3 (2)^2 (2)^1 real(A(3));
(1)^5 (1)^4 (1)^3 (1)^2 (1)^1 real(A(2))])/691200)/length(a);
a=a-da;
%
%----- Velocity - first integration -----
for i=2:length(a)
    v(i)=v(i-1)+(a(i-1)+a(i))*(t(2)-t(1))/2;
end
%
%----- Filtering of the velocity -----
V=fft(v);
dv=(V(1)-det([(-3)^5 (-3)^4 (-3)^3 (-3)^2 (-3)^1 real(V(4));
(-2)^5 (-2)^4 (-2)^3 (-2)^2 (-2)^1 real(V(3));
(-1)^5 (-1)^4 (-1)^3 (-1)^2 (-1)^1 real(V(2));
(3)^5 (3)^4 (3)^3 (3)^2 (3)^1 real(V(4));
(2)^5 (2)^4 (2)^3 (2)^2 (2)^1 real(V(3));
(1)^5 (1)^4 (1)^3 (1)^2 (1)^1 real(V(2))])/691200)/length(a);
v=v-dv;
%
%----- Second integration - displacement -----
for i=2:length(a)
    x(i)=x(i-1)+(v(i-1)+v(i))*(t(2)-t(1))/2;
end
%
%----- Filtering of the displacement -----
X=fft(x);
dx=(X(1)-det([(-3)^5 (-3)^4 (-3)^3 (-3)^2 (-3)^1 real(X(4));
(-2)^5 (-2)^4 (-2)^3 (-2)^2 (-2)^1 real(X(3));
(-1)^5 (-1)^4 (-1)^3 (-1)^2 (-1)^1 real(X(2));
(3)^5 (3)^4 (3)^3 (3)^2 (3)^1 real(X(4));
(2)^5 (2)^4 (2)^3 (2)^2 (2)^1 real(X(3));
(1)^5 (1)^4 (1)^3 (1)^2 (1)^1 real(X(2))])/691200)/length(a);
x=x-dx;
%
end

```

Acknowledgements “This study was financed in part by the Coordenação de Aperfeiçoamento de Pessoal de Nível Superior—Brasil (CAPES)—Finance Code 001.”

References

1. Yi J, Zhang JW, Li QS (2013) Dynamic characteristics and wind-induced responses of a super-tall building during typhoons. *J Wind Eng Ind Aerodyn* 121:116–130
2. Fenerci A, Øiseth O, Rønquist A (2017) Long-term monitoring of wind field characteristics and dynamic response of a long-span suspension bridge in complex terrain. *Eng Struct* 147:269–284
3. Heng L, Yunsheng Y, Shuiming Z, Yongjian C, Dongning L (2011) Baseline correction for digital strong-motion records by using the pre-event portion. *Geodesy Geodynam* 2(1):43–46
4. Akkar S, Boore DM (2009) On baseline corrections and uncertainty in response spectra for baseline variations commonly encountered in digital accelerograph records. *Bullet Seismol Soc America* 99(3):1671–1690
5. Guorui HU, Tao LU (2015) Review on baseline correction of strong-motion accelerogram. *Int J Sci Technol Soc* 3(6):309–314
6. Heng L, Jianchao W, Yunsheng Y, Xiaojun Q (2012) Baseline correction for near-fault ground motion recordings of the 2008 Wenchuan Ms8.0 earthquake. *Geodesy Geodynam* 3(2):60–70
7. Thong YK et al (2002) Dependence of inertial measurements of distance on accelerometer noise. *Measure Sci Technol* 13(8):1163
8. Thong YK et al (2004) Numerical double integration of acceleration measurements in noise. *Measurement* 36:73–92
9. Stiros SC (2008) Errors in velocities and displacements deduced from accelerographs: an approach based on the theory of error propagation. *Soil Dynam Earthq Eng* 28:415–420
10. Han H, Wang J, Meng X, Liu H (2016) Analysis of the dynamic response of a long span bridge using GPS/accelerometer/anemometer under typhoon loading. *Eng Struct* 122:238–250
11. Kim K et al (2018) Structural displacement estimation through multi-rate fusion of accelerometer and RTK-GPS displacement and velocity measurements. *Measurement* 130:223–235
12. Xu Y, Brownjohn JMW, Hester D, Koo KY (2017) Long-span bridges: enhanced data fusion of GPS displacement and deck accelerations. *Eng Struct* 147:639–651
13. Moschas F, Stiros S (2011) Measurement of the dynamic displacements and of the modal frequencies of a short-span pedestrian bridge using GPS and an accelerometer. *Eng Struct* 33:10–17
14. Zheng Z et al (2019) Data fusion based multi-rate Kalman filtering with unknown input for on-line estimation of dynamic displacements. *Measurement* 131:211–218
15. Sekiya H, Maruyama O, Miki C (2017) Visualization system for bridge deformations under live load based on multipoint simultaneous measurements of displacement and rotational response using MEMS sensors. *Eng Struct* 146:43–53
16. Hester D, Brownjohn J, Bocian M, Xu Y (2017) Low cost bridge load test: calculating bridge displacement from acceleration for load assessment calculations. *Eng Struct* 143:358–374
17. Lotfi B, Huang L (2016) An approach for velocity and position estimation through acceleration measurements. *Measurement* 90:242–249
18. Lu Y-S, Wang H-W, Liu S-H (2018) An integrated accelerometer for dynamic motion systems. *Measurement* 125:471–475
19. Zheng W et al (2019) Real-time dynamic displacement monitoring with double integration of acceleration based on recursive least squares method. *Measurement* 141:460–471
20. Kim J, Kim K, Sohn H (2014) Autonomous dynamic displacement estimation from data fusion of acceleration and intermittent displacement measurements. *Mech Syst Signal Process* 42(1–2):194–205
21. Arias-lara D, De-la-colina J (2018) Assessment of methodologies to estimate displacements from measured acceleration records. *Measurement* 114:261–273
22. Ribeiro José Geraldo Telles, Castro Jaime Tupiassú Pinho; Meggiolaro, Marco Antonio. Parameter adjustments for optimizing signal integration using the FFT-DDI method. *J Brazil Soc Mech Sci Eng* 42: 104, 2020
23. Ribeiro, J.G.T.; Castro, J.T.P.; Freire, J.L.F. Some Comments on digital integration to measure displacements using accelerometers, Proceedings of the 17th International Modal Analysis Conference, vol. 3727 (2), pp. 554–559, Kissimmee, Florida, 1999.
24. Ribeiro, J. G. T.; Castro, J. T. P.; Freire, J. L. New improvements in the digital double integration filtering method to measure displacements using accelerometers. Proceedings of the 19th International Modal Analysis Conference, pp 538–542, Orlando, Florida, 2001.
25. Ribeiro, J. G. T.; Castro, J. T. P.; Freire, J. L. Using the FFT-DDI method to measure displacements with piezoelectric, resistive and ICP accelerometers, Proceedings of the 21st International Modal Analysis Conference, Orlando, Florida, 2003
26. Bendat Julius S, Piersol Allan G (2011) Random data: analysis and measurement procedures. John Wiley & Sons

Publisher's Note Springer Nature remains neutral with regard to jurisdictional claims in published maps and institutional affiliations.